Leveraging High Performance Hyperspectral Sensors for the Conservation of Masterworks

J.G. Zeibel
US Army CCDC C5ISR NVESD
UNITED STATES OF AMERICA

Jason.g.zeibel.civ@mail.mil

ABSTRACT

The U.S. Army NVESD has been developing high performance hyperspectral sensors for Army missions for decades. During that time, a partnership was established with the National Gallery of Art to leverage these high value HSI instruments for the characterization and conservation of Masterworks. Works by Picasso, Rembrandt, Van Gogh, Matisse, and many others have been imaged and the resulting data has assisted in their understanding and continued conservation for future generations to enjoy. In this talk, a series of examples from this collaboration are presented, along with some of the lessons learned when using remote sensing equipment for close range, static, indoor imaging.

1.0 INTRODUCTION

The U.S. Army NVESD has been developing high performance hyperspectral sensors for Army missions for decades. Many of these sensor assets are state-of-the-art equipment and can provide high quality spectral data cubes of targets that would be unavailable elsewhere. Since 2007, NVESD has had a partnership with the U.S. National Gallery of Art to leverage these high quality developmental spectral sensor assets for occasional imaging experiments at the Gallery when the sensors are not needed for mission requirements. Some imagery from a few of these imaging experiments is shown in Figure 1.

Much of the previous work in this partnership has focused exclusively on imaging in the reflective bands (visible, near-infrared, and shortwave infrared). This has been highly successful and is described elsewhere [1-7]. In this manuscript, the extension of spectral imaging for masterworks into the longwave infrared (LWIR) will be discussed. The motivation for moving to this spectral channel is summarized in Figure 2. In short, many of the fundamental vibrational and rotational resonances for the materials used in the manufacture of paints, pigments, and binders are located in the LWIR. While the overtones for these transitions can be strong and are observed in the reflective bands, the strength of their signatures is frequently far larger in the LWIR. This can more than make up for the additional experimental complications presented by the need to develop and operate a spectrometer based imaging system capable of achieving a reasonable signal to noise at these longer wavelengths.

One significant complication however when undertaking imagery of masterworks in the thermal infrared is the fact that almost without exception, these works reside in gallery settings that are essentially blackbody cavities. They are maintained at thermal equilibrium with their surrounds, and the amount of illuminating photons that are permitted to fall upon them is tracked and strictly limited. In manuscript, various methodologies that can used to perform LWIR spectral imaging under these conditions are presented, along with some exemplar results. A full treatment of this work from the perspective of an art conservator, including results is also presented elsewhere [[8]].

Figure 1: Images from over a decade of data collection in the partnership between US Army NVESD and the U.S. National Gallery of Art.

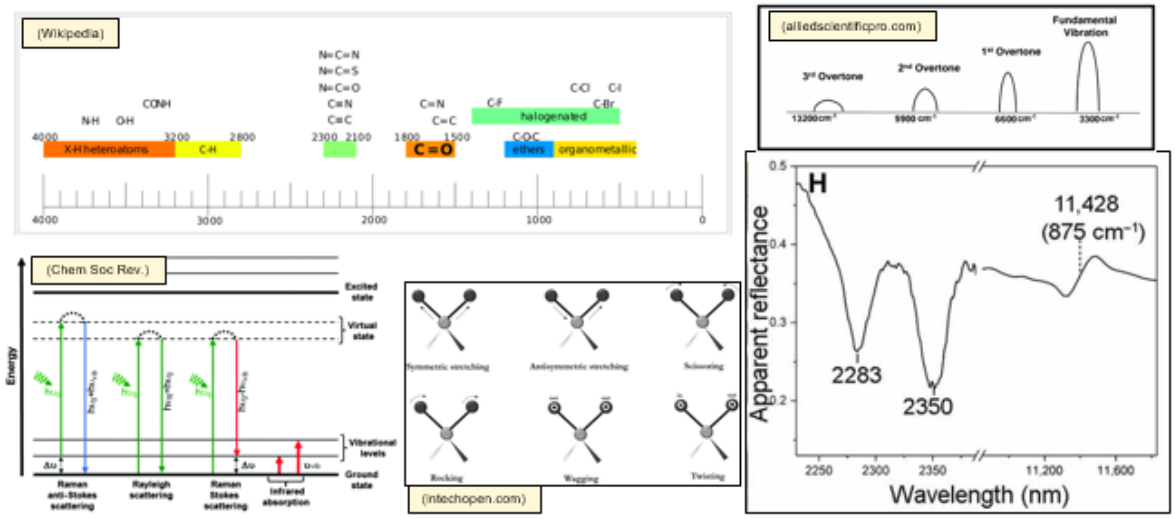

Figure 2: Motivation for using thermal hyperspectral imaging for the study of pigments. Some results taken from [[8]].

2.0 INFRARED RADIOMETRY

Typical airborne or space based infrared remote sensing applications take place under a common set of radiometric conditions. In the case of solid target objects, they are usually at or near the same temperature as the background. Typically, the targets have visibility to some fraction of the sky, and that sky can be treated as having some effective brightness temperature that is likely quite a bit lower than the target temperature. Targets may only have visibility of some fraction of the sky, due to the presence of say obstructions or clouds. In addition, targets may receive illumination from other point sources or diffuse ones.

For ground based infrared remote sensing, the geometric considerations can become more complex, though the basics remain the same. A target of interest has direct line of sight to some large fraction of a cold sky, with which it can exchange photons. The local geometry determines how much of the surrounding hemisphere presents a thermal difference from the target temperature.

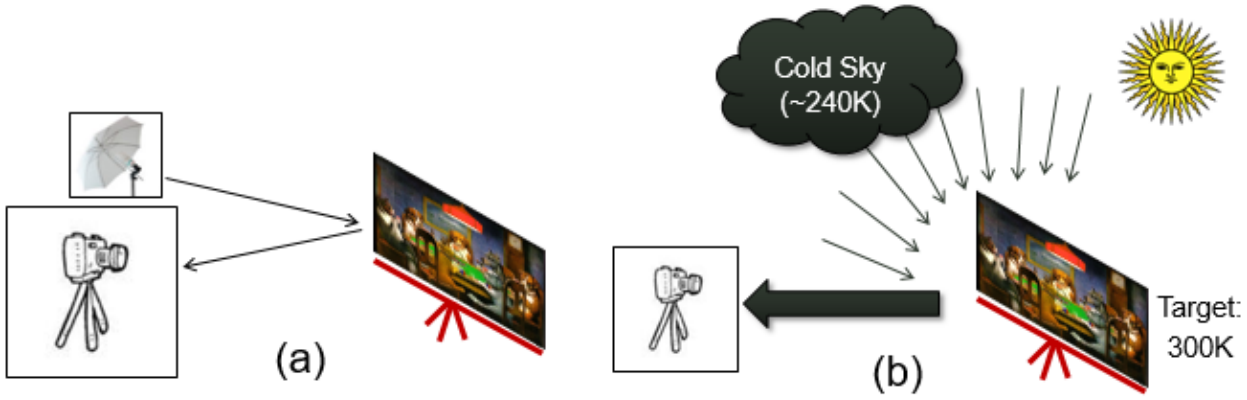

Figure 3:Indoor (a) and Outdoor (b) Imaging Geometries.

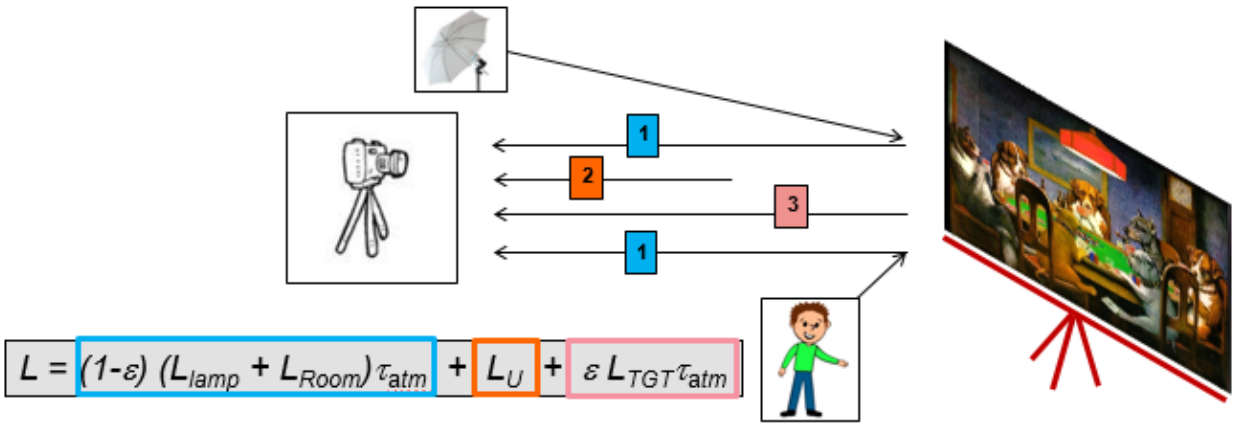

Figure 4: Thermal radiometry with equation, indicating the source of each of the terms.

In the case of indoor thermal imaging, like that encountered at an Art Gallery, there is some level of HVAC system carefully maintaining the local temperature to a very narrow zone, with very small deviations dealt with quickly by a diligent negative feedback thermostat. In this case, everything is mono-thermal: the art, the walls, the ceiling, the floor, etc. Only the presence of people (or other heat sources) standing nearby disrupts the thermal equilibrium. These cases are illustrated Figure 3.

If we consider first just the case of indoor imaging and examine the equation for arriving at-sensor radiance, then we have the situation illustrated in Figure 4. The first term in the equation arises from any sources of radiation present in the room that reflect off of the painting and then arrive at the sensor. Here, this term is further broken down into a term coming from just the thermal background radiation present in the room, and a second term that represents any external "lamp" that may be used. In the strictest sense here, a thermal lamp might be due to a person standing near the painting, or a standard photography quartz-tungsten-halogen (QTH) lamp commonly encountered. Since all radiation represented by this term has reflected off the painting, the radiance is multiplied by (1-emissivity) and by the transmission of the small atmospheric path between the painting and the sensor, both as a function of wavelength. The second term in the radiance equation represents the wavelength dependent path radiance, and the final term represents the emitted thermal energy coming from the painting as a function of wavelength. The goal for solving the radiance equation is to recover the emissivity as a function of wavelength.

If we take the typical gallery case when the painting and room are at the same temperature, and there are no external lamp sources, then all the terms in the radiance equation that contain the emissivity cancel out. In that case, the measured at-sensor radiance is just the blackbody radiance generated by the room. This is the case of a blackbody cavity. Two obvious solutions arise for how to obtain a non-trivial solution to the emissivity: either create a temperature difference between the room and painting (Case #1) or apply some external radiation source (Case #2). For case #1,

$$L = \tau_{atm} L_{room} + L_U + \varepsilon \tau_{atm} (L_{TGT} - L_{room}) \quad (L_{TGT} > L_{room}; L_{Lamp} = 0)$$

And for case #2,

$$L = \tau_{atm} L_{room} + L_U + (1 - \varepsilon) \tau_{atm} (L_{Lamp}) \quad (L_{TGT} = L_{room}; L_{Lamp} > 0)$$

In both cases, a single term remains that contains an emissivity parameter that can be solved for. For the experiments encountered here with imaging of masterworks, the pigments typically have emissivities between 0.9 and 1. Therefore, the emissivity containing term in the first case tends to be significantly larger for a modest temperature difference between the target and room than for the case of reflective thermal imaging from a thermal source. In addition, it is difficult to obtain a Lambertian heat source for thermal reflectance imaging. If the source is non-uniform, then the specularity of the paint surface will lead to hot spots and difficulty in recovering the emissivity in a sufficiently uniform manner. However, there is a significant resistance among conservators to heating up masterwork paintings. Therefore, it was decided to perform a series of experiments to determine the best methodology to recover pigment emissivities without actually heating up a painting.

3.0 DATA COLLECTION

NVESD has developed a number of spectral imaging sensors in their thermal infrared. For this work, the Longwave Advanced Compact Hyperspectral Imager (LACHI) was used to perform measurements (Wavefront Research, Inc., Bethlehem, PA). LACHI is a slit scanning, grism based cryogenic spectrometer that acquires approximately 256 spectral channels of information, with a small amount of band overlap between channels. An example of a LACHI spectral data cube is shown in Figure 5. Only three bands are shown in the Figure, with each mapped to the R, G, and B channels. In order to retrieve the emissivity values of each pixel, a reference channel emissivity separation was run and the results are shown in the lower portion of the Figure.

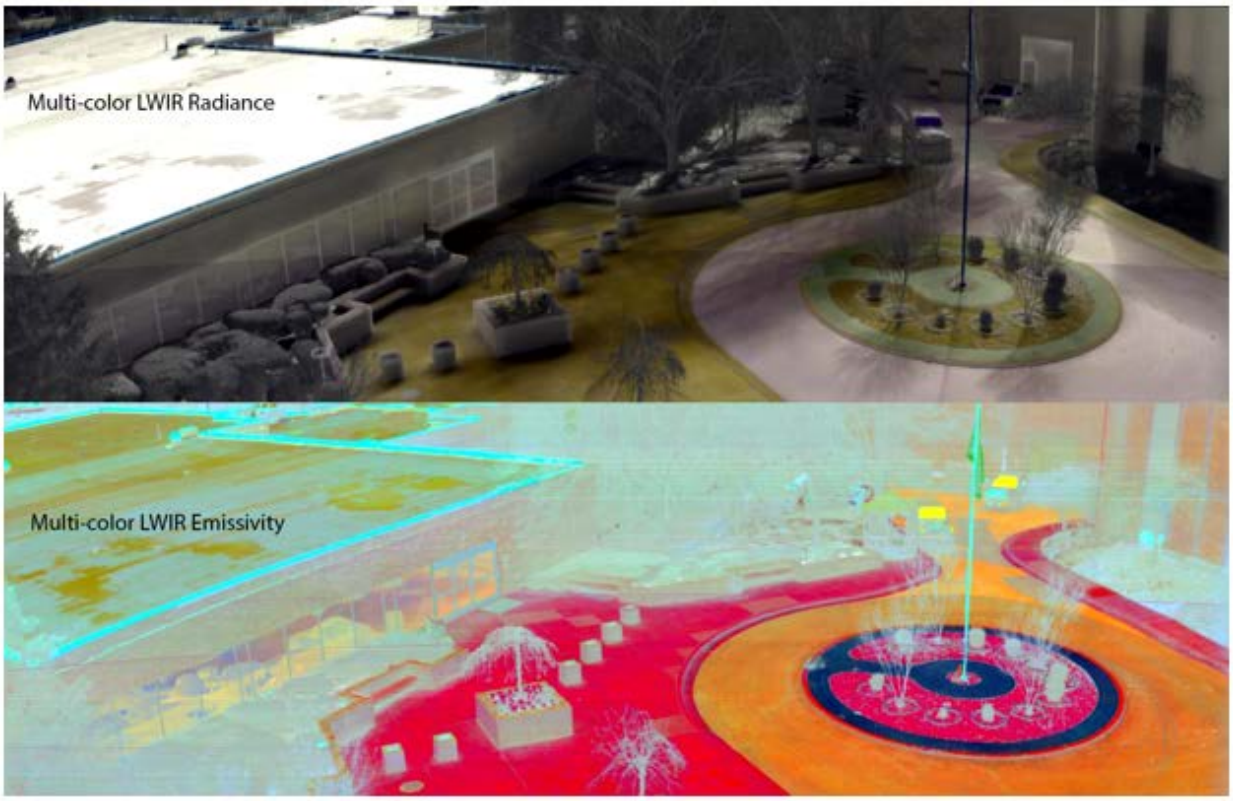

Figure 5: Sample three band radiance image (top) and emissivity image (bottom).

In order to investigate the ability of LWIR spectral imaging to perform pigment identification, a number of sample targets were prepared. These take two forms. The first is a series of wooden boards painted first with a base white coat – typically lead white. The board is then overpainted with a number of small rectangular blocks of period appropriate paints made with various pigments and binders. This provides a very controlled target with easily separable targets of known materials. The other sample target is a sample painting, made with a few known paint samples of interest. This is more realistic test of the LWIR spectral imaging technique as the paints mix, border, overlap, and interact with each other as would be more typical of an actual masterwork.

For a first experiment, it was decided to compare and contrast the ability to recover spectral emissivities of test panels in two methods that can be done without heating the object under study. In the first method, one of the test panels, as well as a test painting were taken outside at NVESD and imaged with LACHI. Several other reference targets were also placed in the scene. These included a wavelength calibration target, a thermal reference source, a sandblasted Aluminium reflectance target, a slab of granite, and a Silicon Carbide sample. A photograph of this setup, along with a three-band radiance image from the LACHI data cube is shown in Figure 6.

After the outside data was acquired, then the setup was replicated inside a lab at NVESD, but with the addition of a large heat lamp that was placed approximately 2m from the test panel. The test panel was allowed to equilibrate with the ambient environment and the heat lamp was turned on moments before data collection commenced. The heat lamp was then turned off as soon as the LACHI collection was completed. Typical LACHI scan times are only a few seconds, so no measurable heating of the painting occurred during the indoor heat-lamp based testing.

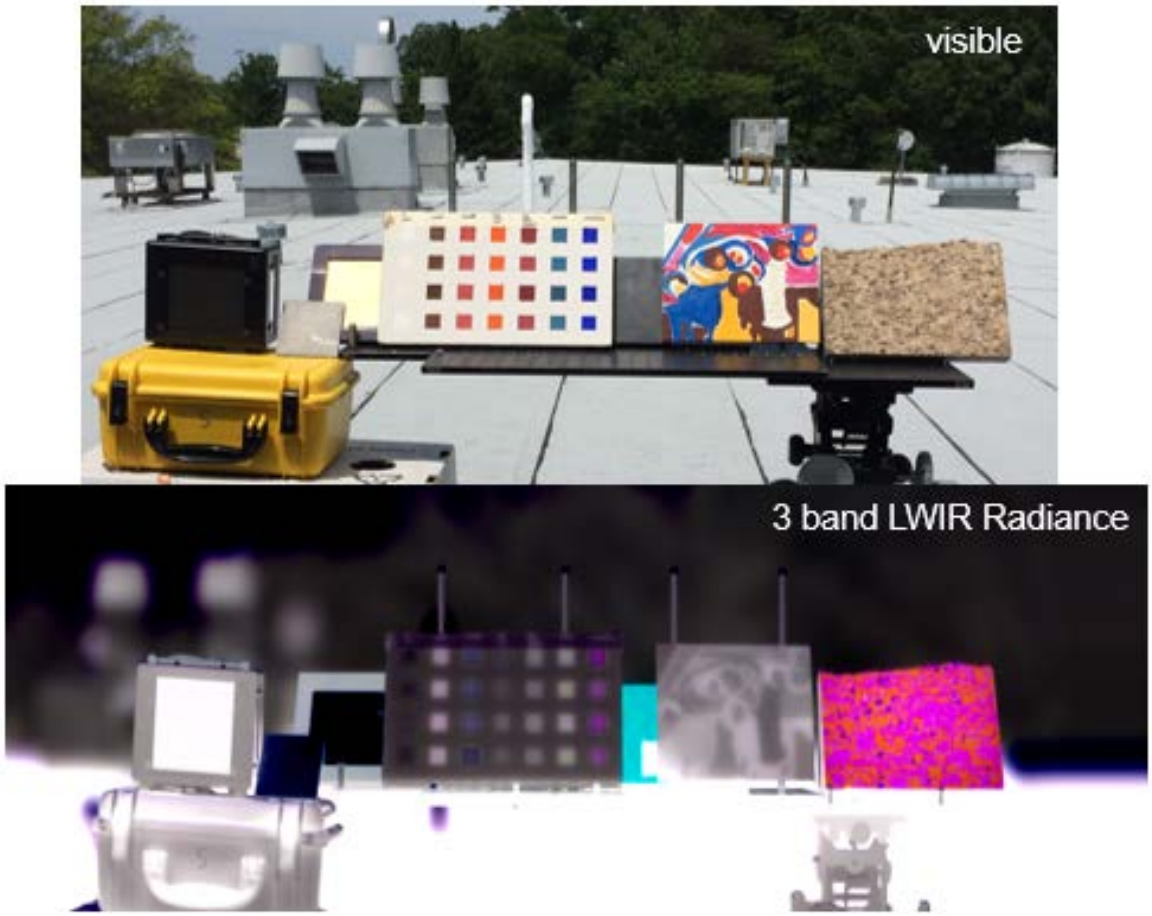

Figure 6: Visible and three band thermal radiance images of a granite panel, a painting, a painted test panel, and calibration targets.

Once the data from the two cases was acquired, regions of interest were selected for one row of painted samples on the test panel. Radiance spectra were then recovered for each ROI. An example is shown in Figure 7. The radiance spectra are dominated by the Planck curves, though the spectral emissivity variations are observable on top of the blackbody curves. Also of note is some specular reflection from the indoor with heat lamp imagery. Placement of the lamp was difficult to optimize to achieve uniform illumination on the target panel, while avoiding very strong specular reflections when the lamp was near normal to the target panel.

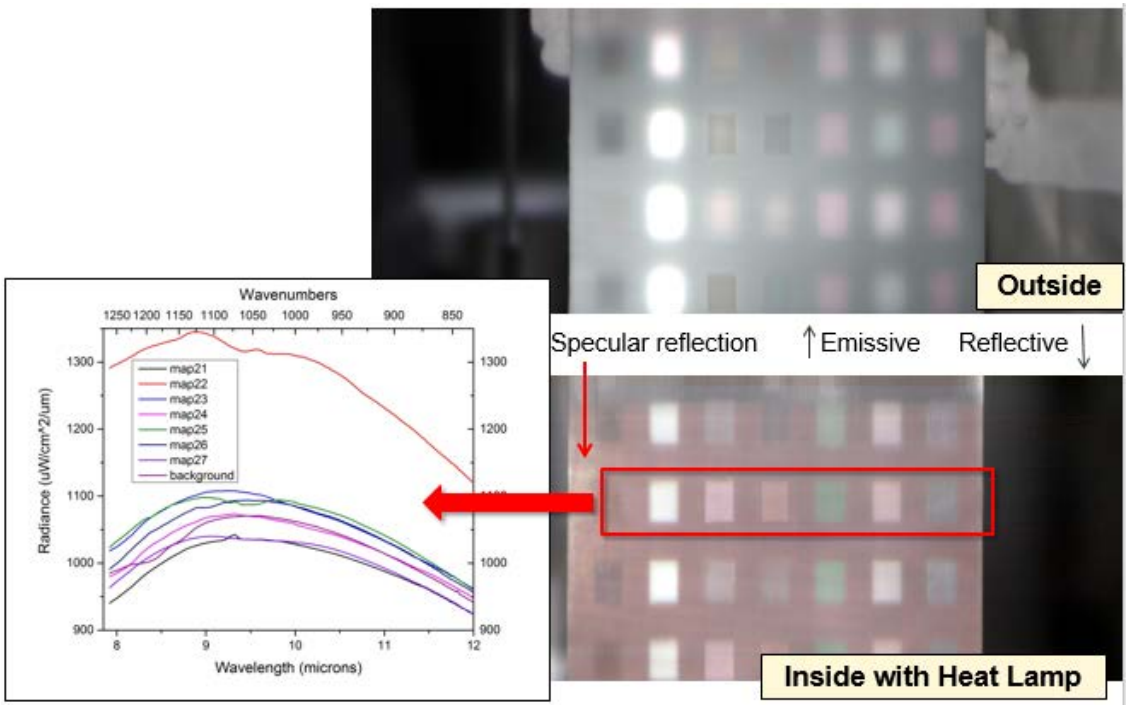

Figure 7: Radiance images from outside (top) and inside with a heat lamp (bottom). The spectra are shown from one line of test paints at left.

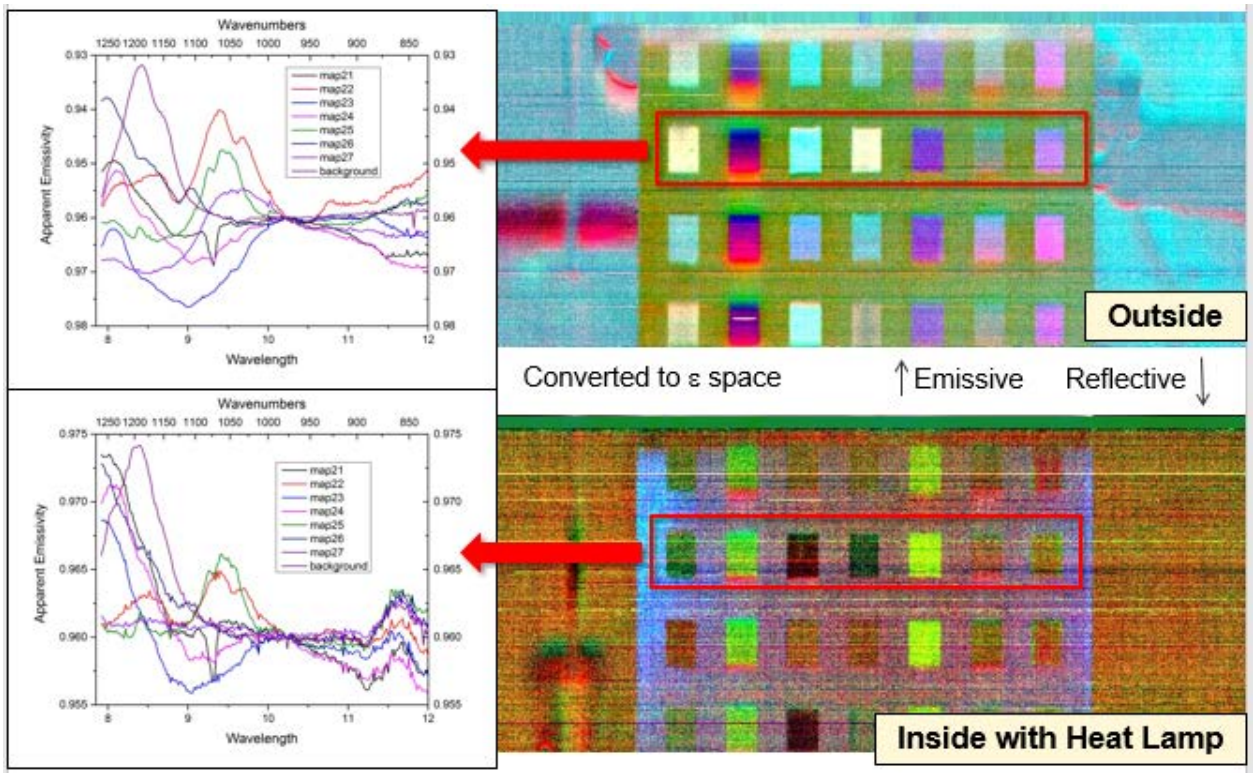

Figure 8: Emissivity recovery using a simple reference channel normalization of the (top) outside imaging experiment and (bottom) indoor imaging experiment. Note the spectra are similar from the highlighted row, though the indoor reflective imaging is noisier.

A temperature / emissivity separation was performed on the data shown in Figure 7, and the results are shown in Figure 8. In general, the noise is significantly higher on the heat lamp based image data. This is likely due to the much smaller contribution to the at sensor radiance from the reflected imaging setup than for the emitted energy case with the cold sky. In addition, there is likely some error introduced by the spatial non-uniformity of the illumination of the heat lamp. Nevertheless, there is good qualitative agreement between the recovered emissivity spectra of all the paints on the test panel.

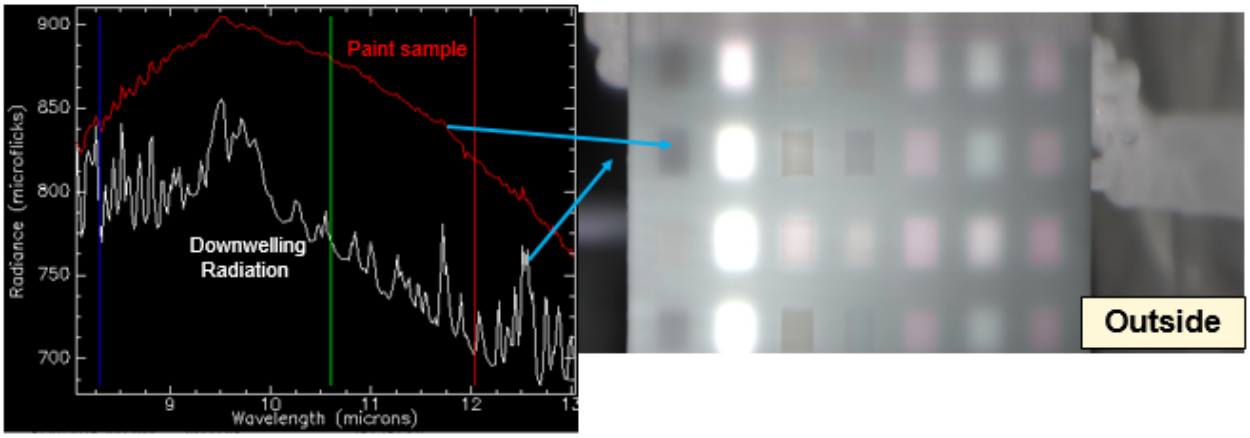

Figure 9: Radiance spectra for outdoor imaging. Note the presence of many atmospheric peaks in the sky spectrum (white), and how these are manifest in the paint sample spectrum (red).

One drawback of performing outdoor imaging with a cold sky is the need to carefully compensate for the very complex spectral illumination presented by the atmospheric absorption. In Figure 9, an example pixel is shown in white that sees the direct illumination of the sky. The atmospheric transmission of the sky is a complex, though well understood problem that presents a downwelling source with high spectral variability. Many methods exist to compensate for these atmospheric absorption features, though none of them is perfect at removing all traces of atmospheric spectral variability. Since the effect of the emissivity variations in the paints on the radiance spectra are typically much smaller than the atmospheric variability in illumination, it can be difficult to recover the spectral emissivity of these targets without having atmospheric artifacts contaminate the spectra. From this series of experiments, it appears that the best imaging geometry that avoids heating the target would be to image outside with a cold sky that somehow is devoid of any of the persistent atmospheric absorption lines.

4.0 INDOOR COLD TUNNEL EXPERIMENT

Based on the lessons learned from the test panel imaging and the radiometry, the imaging goals were as follows: (1) do not heat the target, (2) achieve a delta T between target and background, (3) avoid the presence of atmospheric absorption features in the data, and (4) keep art conservators happy by not bringing the target painting outside where it might suddenly rain or have a bird fly by without warning. In order to meet all of these goals, a new experiment was designed to place the target painting near a reflective cold box, where it sees a controlled hemisphere that is maintained at a temperature significantly lower than room ambient. This was done by placing a large stack of foam in an insulated tray and soaking the foam repeatedly with liquid Nitrogen. Next, a three sided tunnel made of polished aluminium was introduced over the LN2 soaked foam and between the LACHI sensor and the paintings under test. The result of this setup is that nearly the full hemisphere located “above’ the painting, or normal to the painting sees the LN2 soaked foam and a significantly colder temperature than the room ambient. There was approximately 5cm between the end of the Aluminum tunnel and the easel the painting was mounted to. During testing, the temperature of the painting

was monitored with an infrared non-contact thermometer. The target painting temperature was observed to be within 2C of the room ambient at all times. Figure 10 shows a picture of the setup, as well as some example ray traces of emitted energy from the painting under test – both from the side and the end of the cold tunnel.

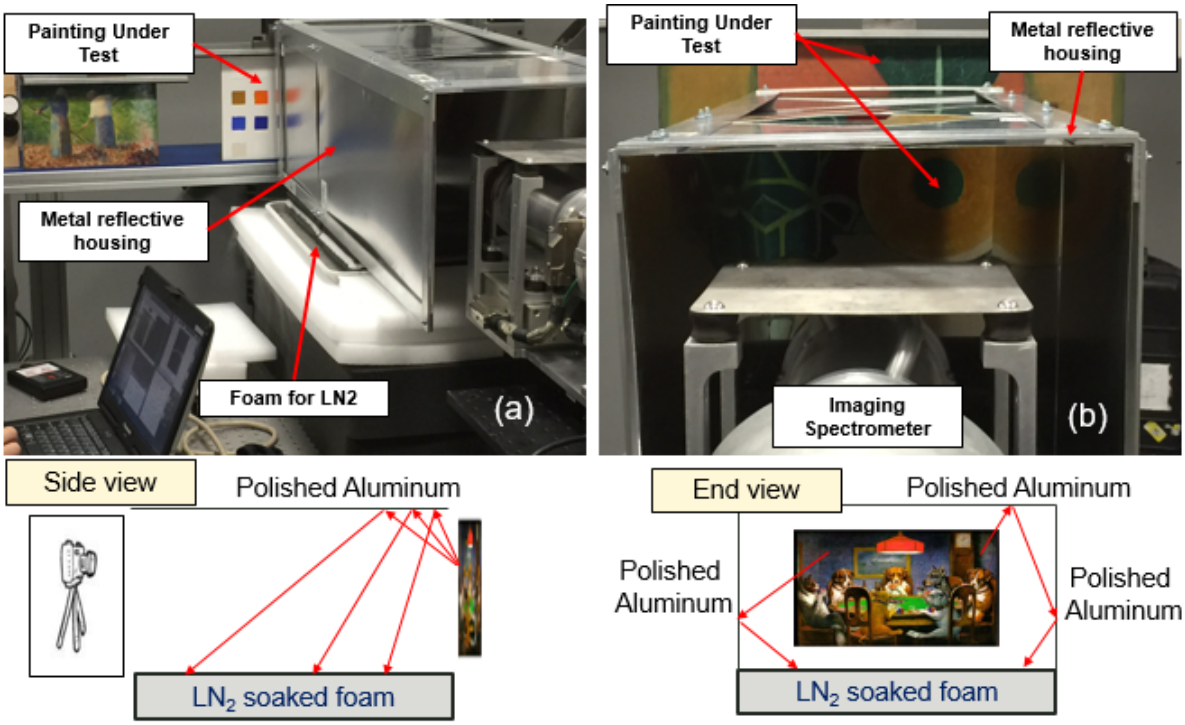

Figure 10: (a) Side view and (b) End view of the initial cold tunnel imaging setup.

A three band composite image from a sample data cube of the test painting done in the cold tunnel geometry is shown in Figure 11. The slit is vertical in this geometry and is scanned across the image from left to right. Note that the painting is larger than the opening at the end of the cold tunnel, so when the scan reaches the edge of the box, the reflection of the painting is then seen in the data. This shows the effectiveness of the Aluminium sided box to reflect energy down to the cold LN_2 foam. In this radiance image, many features are seen that are not easily visible in the painting (shown in the inset). In addition, the emissivity spectra can easily be recovered from the data in Figure 11, almost entirely free from the effects of atmospheric absorption lines.

Figure 11: Three band radiance imagery from the cold tunnel imaging setup.

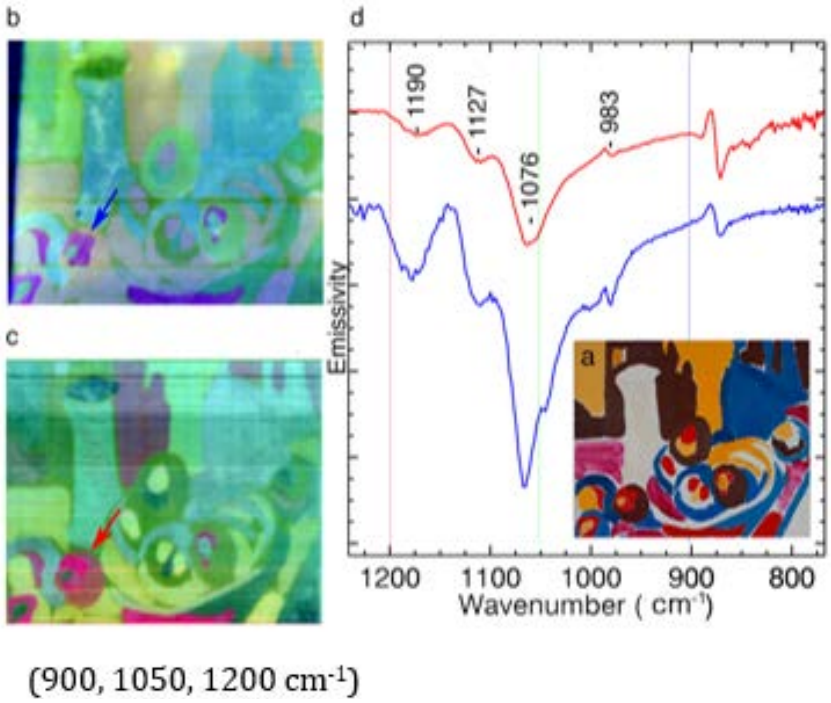

Figure 12: Comparison of the test painting (a) from both the indoor imaging cold tunnel experiment (b) and the outdoor imaging experiment (c). Spectra from the pigment shown in the arrows is plotted in (d), with the red curve corresponding to the cold tunnel experimental setup and the blue curve corresponding to the outdoor imaging.

In order to evaluate the effectiveness of this imaging geometry, the recovered emissivity data from the cold tunnel geometry is compared with that obtained from the outdoor cold sky imaging geometry. This is shown in Figure 12. In the Figure, two curves of recovered emissivity are shown from one site in the test painting. The red curve is the recovered emissivity from the cold tunnel experiment, while the blue curve shows the emissivity from the outdoor imaging with a cold sky. The spectral features are very similar in the two cases, with a bit more noise on otherwise deeper features seen on the outdoor imaging data. The spectral positions for several key features are called out.

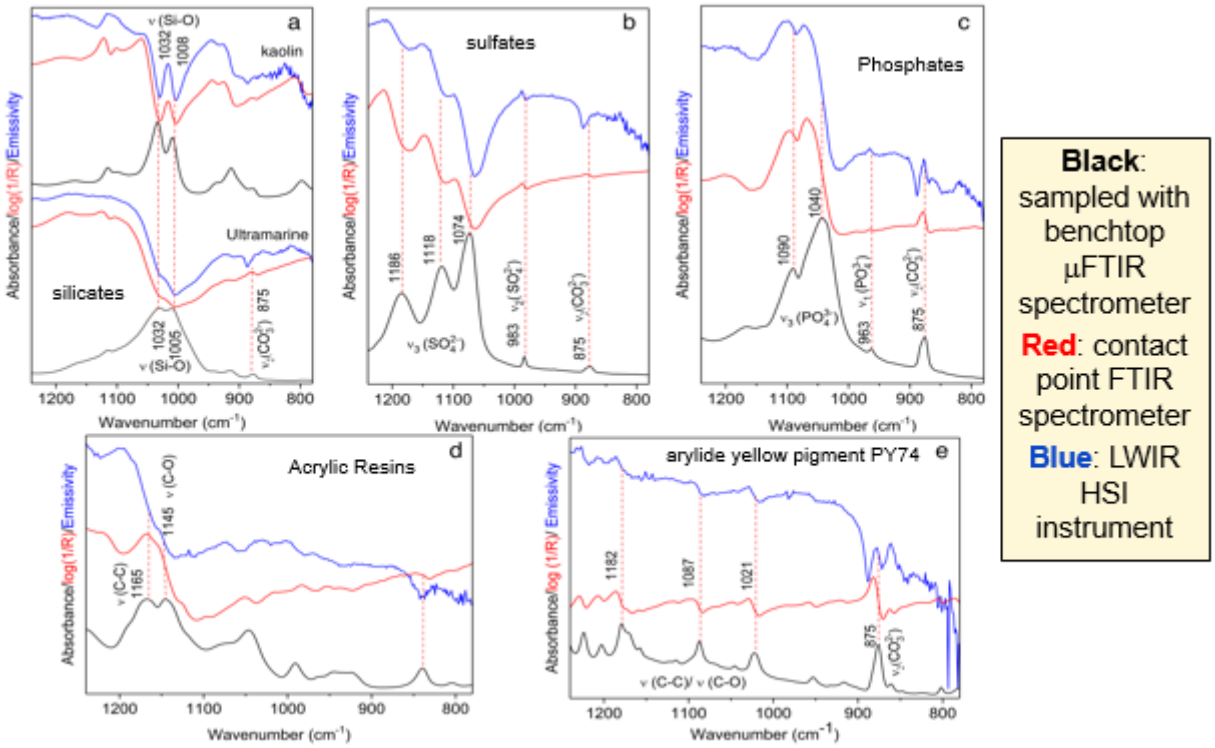

Figure 13: Comparison of the LWIR HSI data (blue), with that of a point contact FTIR reflectometer (red) and a benchtop, destructively sampled FT-IR (black) for five different pigment materials.

The next step in the data analysis for this sensing modality is to compare and hopefully confirm the recovered spectral signatures with those obtained on the same paints by different sensors using more traditional techniques. This was performed in two ways: contact point spectroscopy and destructive sampling. In contact point spectroscopy, an active source FT-IR is brought into contact with the spot to be measured on the painting. A small cavity is created over that spot and the energy from a glowbar source is reflected off the painting and measured in a detector. Reflectivity spectra are recovered through an interferometer and FFT. In destructive sampling, a small sample (typically micrograms) of material is scraped from the surface of the painting at the site of interest. This sample is diluted and analyzed in a bench-top level FT-IR, where absorbance through the sample is measured. Both of these techniques are industry standard practices and yield good confirmation of material identification.

The LACHI data analysis on the test painting and test panels was confirmed with both the contact point FT-IR and the sampling analysis. The results are shown in Figure 13. Five different classes of pigments were measured. The agreement is best within the silicates and sulfates, though features are identified in all paints examined in this work. While the signal to noise on the LAHCI HSI data is not as good as it is with the other two measurement techniques, neither of the other approaches is easily scalable to measure entire paintings,

and the time required to try these is orders of magnitude greater than the few seconds that it takes to acquire a hyperspectral data cube with the LACHI sensor.

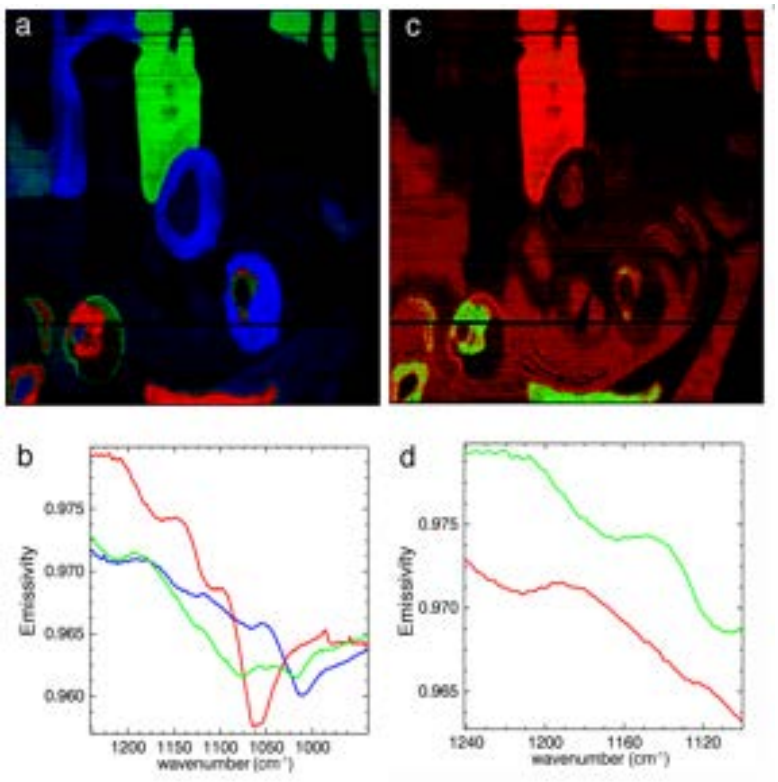

Figure 14: Spectral end-members from the LWIR HSI measured data for five different pigments. Panels (a) and (c) show the relative abundances and locations of each of the endmembers.

As an illustration of the added utility of the HSI sensing modality over point sampling techniques, the spectral data cube acquired with the cold tunnel imaging was whitened into principal component space. Spectral endmembers were identified from the image and their locations were then mapped out on the artwork. The results of this analysis is presented in Figure 14. In the Figure, five different pigments are identified and their respective locations in the figure are easily identified. Panels (a) and (b) show $BaSO_4$ in oil and alkyd paints (red), silicate in oil and alkyd paints (blue), and silicate in acrylic paints (green). The spectra in (d) show the mapping of all regions where acrylic paint was used (red) as opposed to $BaSO_4$ in oil and alkyd paint (green) [[8]]. This information can be critical to art conservators as they attempt to conserve, stabilize, restore, or attribute a work of art.

All of the work presented thus far has been on test panels and test paintings. While these articles were produced using period appropriate materials in relevant combinations and with known techniques, it is crucial to evaluate this sensing modality with actual artwork. In Figure 15, Edward Steichen's Study for "Le Tournesol (The Sunflower)" is analyzed in the same method as the previous test painting examples. It was scanned with the LACHI sensor in the indoor cold tunnel geometry. Spectral endmembers have been recovered and are shown in the right panel of the Figure. The mapping of these endmembers back to the original painting is also shown in (b). From this data, the blue can be identified as lead sulfate ($PbSO_4$), the brown as kaolin, and the dark yellow on the vase as $CaCO_3$.

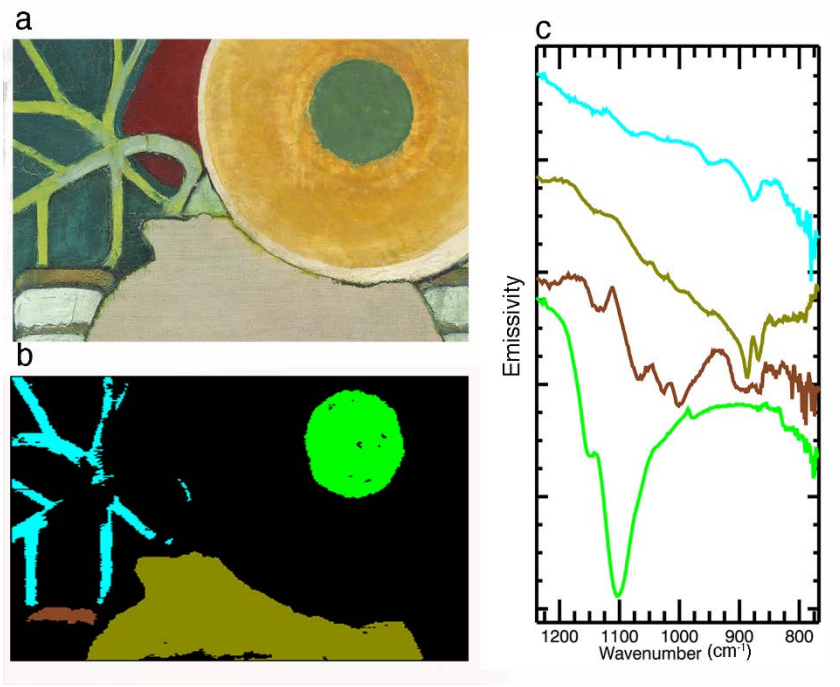

Figure 15: Color detail of Edward Steichen's Study for "Le Tournesol (The Sunflower)" (a); gift of Joanna T. Steichen © Estate of Edward Steichen, and map (b) of the spectral endmembers (c) [[8]].

5.0 CONCLUSIONS AND FUTURE WORK

While the LN_2 cold tunnel appears to have worked quite well for this experiment, there are improvements in the setup that were needed in order to make this technique more repeatable. First of all, the foam temperature was constantly changing and therefore the signal was varying over time. Ideally, a steady state condition is desired for all imaging conditions. Next, a fair amount of ambient room signature was still visible around the camera that wasn't being reflected by the box walls. Most frustrating was the relatively small size accessible in this setup. Only about a 12" x 12" size square could be studied at a time.

In order to improve on this technique, a new cold tunnel is being fabricated that will incorporate some of these lessons learned. Some photographs of this tunnel are shown in Figure 16. Instead of highly reflective walls, all four sides of the new tunnel are highly emissive and will be held at or around 0C. Instead of LN_2 as the cold source, the new tunnel uses a steady state liquid chiller with refrigerated ethylene glycol. The glycol is pumped through a close cycle channel that flows through all the walls. In order to prevent frosting or condensation forming on the walls, a laminar flow system was developed that will create a smooth flow of dry nitrogen across the surface of each wall. In the back of the tunnel, a custom fit reflective plate is installed that just fits around the lens of the imaging camera. The entire unit is insulated and mounted approximately 5cm from a sliding easel system that will permit rapid, repeatable placement of the object under test. It is anticipated that measurements with the new cold tunnel will be much more repeatable and quantitative than with the LN_2 soaked foam.

Figure 16: Images of the next generation of the indoor cold chamber.

In conclusion, LWIR spectral imaging has been demonstrated to be a viable tool for art conservators in the preservation of masterworks. It provides a combination of spectral identification and spatial mapping that is not possible through other imaging modalities. The radiometry equations dictate that LWIR spectral imaging done in an indoor laboratory environment can be challenging due to the required temperature difference. A workable solution for this was presented and is being improved on for future imaging experiments.

6.0 ACKNOWLEDGEMENTS

The author would like to thank Dr. John Delaney and Ms. Katheryn Dooley of the National Gallery of Art for their collaboration and assistance.

7.0 REFERENCES

[1] John K. Delaney, Mathieu Thoury, Jason G. Zeibel, Paola Ricciardi, Kathryn M. Morales and Kathryn A. Dooley, "Visible and infrared imaging spectroscopy of paintings and improved reflectography" , Heritage Science epub 2016 Mar 16. http://heritagesciencejournal.springeropen.com/articles/10.1186/s40494-016-0075-4

[2] Van der Snickt, G., Martins, A., Delaney, J., Janssens, K., Zeibel, J., Duy, M., McGlinchey, C., Driel, B.V., Dik, J.: Exploring a hidden painting below the surface of Renee Magritte's Le Portrait. Applied Spectroscopy **70**(1), 57-67 (2016).

[3] K. A. Dooley, S. Lomax, J. G. Zeibel, C. Miliani, P. Ricciardi, A. Hoenigswald, M. Loew and J. K. Delaney, "Mapping of egg yolk and animal skin glue paint binders in Early Renaissance paintings using near infrared reflectance imaging spectroscopy", Analyst, 8 May 2013, DOI: 10.1039/c3an00926b.

[4] P. Ricciardi, J.K. Delaney, M. Facini, J.G. Zeibel, M. Picollo, and M. Loew, "Near Infrared Reflectance Imaging Spectroscopy to Map Paint Binders in situ on Illuminated Manuscripts", Angew Chem Int Ed Engl. 2012 Jun 4;51(23):5607-10.

[5] J.K. Delaney, J.G. Zeibel, M. Thoury, Roy Littleton, Kathryn Morales, E. Rene. de la Rie and Ann. Hoenigswald, "Visible and Infrared Imaging Spectroscopy of Picassos's Harlequin Musician: Mapping and Identification of Artist Materials in situ", Applied Spectroscopy 64, No. 6, (2010).

[6] John K. Delaney; Jason G. Zeibel; Mathieu Thoury; Roy Littleton; Kathryn M. Morales; Michael Palmer; E. René de la Rie. "Visible and infrared reflectance imaging spectroscopy of paintings: pigment mapping and improved infrared reflectography". Optics for Arts, Architecture, and Archaeology II. Proceedings of the SPIE, Volume 7391, pp. 739103-739103-8 (2009).

[7] F. Casadio, L. Toniolo, The analysis of polychrome works of art: 40 years of infrared spectroscopic investigations. *J. Cult. Herit.* **2**, 71–78 (2001).

[8] F. Gabrieli, K. A. Dooley, J. G. Zeibel, J. D. Howe, J. K. Delaney, Standoff mid-infrared emissive imaging spectroscopy for identification and mapping of materials in polychrome objects. *Angew. Chem. Int. Ed.* **57**, 7341–7345 (2018).

[9] Gabrieli *et al*., *Sci. Adv.* 2019; **5** : eaaw7794 23 August 2019